

# Effect of metal (Ti) interlayer on fracture toughness of TiN thin films

Nidhin George Mathews<sup>1,a</sup>, Alosious Lambai<sup>1</sup>, Marcus Hans<sup>2</sup>, Jochen M. Schneider<sup>2</sup>, Gaurav Mohanty<sup>1</sup>, Balila Nagamani Jaya<sup>3,a</sup>

<sup>1</sup> *Materials Science and Environmental Engineering, Faculty of Engineering and Natural Sciences, Tampere University, Tampere 33014, Finland*

<sup>2</sup> *Materials Chemistry, RWTH Aachen University, 52074 Aachen, Germany*

<sup>3</sup> *Department of Metallurgical Engineering and Materials Science, Indian Institute of Technology Bombay, Mumbai 400076, India*

<sup>a</sup> *Corresponding authors: nidhin.mathews@tuni.fi; jayabalila@iitb.ac.in*

## Abstract

Titanium Nitride (TiN) is widely used as a protective coating due to its high hardness, but suffers from inherent brittleness and low fracture toughness, limiting its applicability. The layering of Titanium Nitride films with metallic Titanium (Ti) improves the overall fracture behavior of system by modifying the crack driving force due to elastic-plastic mismatch between the layers. Microcantilever fracture tests were carried out on bilayer (Ti-TiN, TiN-Ti) and trilayer (Ti-TiN-Ti) systems to determine the fracture toughness and study the fundamental crack growth behavior. The initiation fracture toughness in bilayer system with crack in Ti layer is almost 70% higher when compared to crack in TiN layer. In Ti-TiN bilayer the crack propagated catastrophically post linear elastic deformation, whereas the crack was arrested at the TiN/Ti interface in both TiN-Ti and Ti-TiN-Ti systems due to plastic energy dissipation in the Ti layer. Incorporation of crack tip plasticity due to the metallic layer increased the total resistance to fracture by around eight times compared to the Ti-TiN bilayer.

**Keywords:** Titanium Nitride, Multilayer thin films, Fracture toughness, Microcantilever bending, Crack tip plasticity

## 1 Introduction

Titanium Nitride (TiN) provides excellent hardness, mechanical strength, and chemical stability which finds applications in harsh or extreme environmental conditions. It has been used extensively as a hard coating material for different applications in cutting tool manufacturing, tribology, hydrogen barriers, oxidation and corrosion resistance coating [1]. Even though TiN possess high strengths, the material is inherently brittle and has low fracture toughness. Combining the TiN coating with a metallic Titanium (Ti) layer further has been

shown to improve the durability of the multilayered systems by enhancing its fracture resistance [2–6]. Tailoring the layer thickness of the Ti-TiN multilayer system changes the residual stress state, along with bringing an elastic-plastic mismatch across the interface, which in turn contributes to the improvement in mechanical properties such as hardness, elastic modulus, and fracture toughness of layered systems [7–9].

Several previous studies have been carried out to determine the fracture behavior of Ti-TiN multilayers systems using indentation-based techniques [3–5]. They showed an improvement in the fracture resistance of the system with the increase in the layer thickness and thickness ratio of the Ti (ductile) layer, consequently with a drop in hardness. But these tests do not provide any insights into the nature of the fracture, since the fracture path under a complex tri-axial stress state of an indenter is unknown. Notched microcantilever bending has been widely used to study the crack growth behavior of free standing and multilayered films, as one can determine the contribution of individual layers and interfaces towards crack propagation [10,11]. Fracture toughness ( $K_{IC}$ ) of sputtered TiN monolayer layer is reported to lie in the range of 1.2 – 3.0 MPa.m<sup>0.5</sup>, which failed in a linear elastic brittle manner [12–14]. In a specific magnetron sputtered film, the addition of ductile Ti layer was shown to provide toughening, increasing the fracture toughness to 3.2 MPa.m<sup>0.5</sup> for a 50 layer Ti-TiN multilayer, almost double that of monolayer TiN films which showed a fracture toughness of 1.4 MPa.m<sup>0.5</sup> [6]. Crack growth under mode I loading conditions was found to be straight, cutting across the layers, following the inter-columnar boundaries of the sputtered films. The Ti/TiN interface was found to be strong and prevented any crack deflection along the interface. The elastic-plastic mismatch between the Ti and TiN layers was quantified in terms of changes in crack driving force, which was accounted for in their modified stress intensity factor solutions [6]. In addition, the compressive residual stresses (up to 8 GPa) which developed due to the layering may also have imparted additional toughening, which could not be separately discerned. However, the sputtered Ti layer while independently showed some degree of crack tip plasticity and non-linear deformation behavior, did not show any expression of plasticity when sandwiched between TiN in the multilayer systems. The possible reasons for this suppression of crack tip plasticity is due to the constraint on both sides of the Ti layer by the harder and stiffer TiN, and the inability to accommodate plasticity in individual Ti layer due to its low thickness (80 nm). However, there was uncertainty due to the low stiffness of the indentation-micromechanical loading system, which could have overloaded the microcantilevers, leading to abrupt, catastrophic fracture [6].

The objective of this study is to address these open questions on the effect of elastic-plastic mismatch between the layers and its relative position with respect to crack tip on promoting crack tip plasticity and prevention of catastrophic fracture in these systems. Notched microcantilevers of trilayered Ti-TiN-Ti, and two bilayered Ti-TiN and TiN-Ti (micromachined out of the same Ti-TiN-Ti trilayer sputtered films) are the focus of the study. The crack tip position is varied to alternately determine the effect of an elastically and plastically stiffer (TiN) and a compliant (Ti) layer ahead of the interface, followed by the overall fracture behavior of the tri-layer system. The presence of a ductile, softer, metallic layer is expected to a) modify the crack driving force due to elastic-plastic shielding/anti-shielding at the interface, b) crack tip blunting c) crack closure due to compressive residual stresses. Finite element simulations are performed to estimate the crack driving force variation with the specific conditions of bilayer and trilayer systems.

## **2 Materials and methods**

### ***2.1 Thin film deposition and microstructural characterisation***

Multilayer thin film samples of Ti and TiN were synthesised using a magnetron sputtering system on Si (100) substrate. The trilayer film system of Ti-TiN-Ti was deposited with Ti as the first layer on Si, with the aim of depositing approximately 1  $\mu\text{m}$  thickness of each layer. Details about the deposition parameters are described in a previous work [6]. The structural characterisation of the deposited thin film sample was performed using grazing incidence X-ray diffraction (GI-XRD) studies (Malvern Panalytical Empyeron, United Kingdom). XRD scans were performed on the film at an incidence angle of  $10^\circ$  using  $\text{CuK}\alpha$  radiation of wavelength ( $\lambda$ ) 0.154 nm, operated at 40 kV voltage and 30 mA current. Focussed ion beam (FIB) cross-sectioning was performed on the Ti-TiN-Ti trilayer system to determine individual layer thickness. The  $\text{Ga}^+$  ion current at 300 pA at an accelerating voltage of 30 kV was selected for the cross-section milling. The milled region was imaged in ion channeling contrast in a dual beam SEM (Zeiss Crossbeam 540, Germany) using the 50 pA ion current to visualise the layers.

### ***2.2 Microcantilever sample preparation and fracture testing***

Micromechanical fracture testing of the thin film samples was performed using single-edge notched microcantilever bend tests. Free standing microcantilevers were fabricated at the edge of the specimen using FIB milling (Zeiss Crossbeam 540, Germany). Ion currents of 15 nA, 3 nA and 0.3 nA at 30 kV operating voltage were selected for the coarse, intermediate and fine milling steps respectively. The front and back sides of the cantilevers were fine polished at an additional tilt angle of  $\pm 1.5^\circ$  to maintain uniform rectangular cross-section of the beam. The

geometrical dimensions of the cantilever, length ( $L$ ): thickness ( $W$ ): width ( $B$ ) was maintained at constant ratio of 4.5: 1: 1 for all cases. Notches were milled at a distance ( $x/W$ )  $\sim 2 \mu\text{m}$  from the fixed end of the cantilever using 10 pA milling current. Notch depth to width ratio ( $a/W$ ) was maintained in the range 0.25 - 0.3 in all test cases with the notch positioned entirely in the top layer. These geometrical dimensions and the loading position were considered so as to maintain a dominant mode I loading conditions for fracture in the cantilevers [15]. Fig. 1a - Fig. 1c shows the images of microcantilevers of each film-substrate conditions: a) Ti-TiN bilayer ( $W = 2.4 \mu\text{m}$ ) with the notch in the Ti layer, b) TiN-Ti bilayer ( $W = 2.4 \mu\text{m}$ ) with the notch in the TiN layer and c) Ti-TiN-Ti trilayer ( $W = 3.7 \mu\text{m}$ ) with the notch in the Ti layer. The layer which is mentioned first is on the top surface of the cantilever. It should be reiterated that the bilayer TiN-Ti and Ti-TiN cantilevers were prepared from the trilayer film by FIB milling the top and bottom layers respectively. In these cases, a plastic zone size ( $r_y$ ) of  $\sim 300 \text{ nm}$  was estimated using the Irwin process zone model, according to Eq. 1, considering  $K_{IC} = 3 \text{ MPa}\cdot\text{m}^{0.5}$  and  $\sigma_y = 2.1 \text{ GPa}$ , where  $\sigma_y$  is the nominal yield strength in bending, derived from microcantilever bend tests [6]. The estimated plastic zone size is  $\sim 10$  times lower than the cantilever dimensions ( $B, W$ ) ensuring plane strain conditions of fracture.

$$r_y = \frac{1}{2\pi} \left( \frac{K_{IC}}{\sigma_y} \right)^2 \quad \text{Eq. 1}$$

The microcantilever fractures tests were performed using an *in situ* displacement controlled nanoindenter (Alemnis AG, Switzerland) inside a SEM (Zeiss Leo, Germany). A diamond wedge indenter tip (Synton MDP, Switzerland) of  $10 \mu\text{m}$  length and  $100^\circ$  opening angle was used for loading the cantilevers, to ensure line contact and prevent indentation based deformation [16]. Fracture experiments were conducted in displacement control mode with tip travel speed of  $50 \text{ nm/s}$ . In such displacement-controlled tests, crack propagation results in distinct load drops. The displacement values recorded during the tests were then corrected for the machine compliance to get the actual displacement of the cantilever. At least three microcantilevers were tested for each condition. Initiation fracture toughness ( $K_{IC}$ ) of the tested films based on linear elastic fracture mechanics (LEFM) was calculated from the critical load ( $P_c$ ) *i.e.* maximum load at which crack initiation occurs, using Eq. 2 [10] and Eq. 3 [15], assuming linear elastic behavior until then.

$$K_{IC} = \frac{P_c L}{B W^{1.5}} f\left(\frac{a}{W}\right) \quad \text{Eq. 2}$$

$$f\left(\frac{a}{W}\right) = -3.15 + 72.85 \left(\frac{a}{W}\right) - 188.51 \left(\frac{a}{W}\right)^2 + 202.61 \left(\frac{a}{W}\right)^3 \quad \text{Eq. 3}$$

To quantify the fracture behavior in the non-linear elastic-plastic regime of fracture (*i.e.* post the first load drop), crack tip opening angle (CTOA) was used as the fracture resistance parameter of material. CTOA is defined as the included angle between two faces of the opening crack surfaces measured with crack tip as the vertex (as shown in Fig. 1d). The overall fracture resistance ( $J_R$ ) is evaluated considering the total area under load-displacement curve using Eq. 4 [17], according to elastic plastic fracture mechanics (EPFM).

$$J_R^{(i)} = \frac{\eta A_{tot,i}}{B(W-a_i)} \quad \text{Eq. 4}$$

where,  $A_{tot,i}$  is the total area under the load-displacement curve at instant  $i$  (or more specifically the total work done during the event),  $\eta$  is a shape factor equal to 2 for cantilevers, and  $a_i$  denotes the crack length at instant  $i$ .

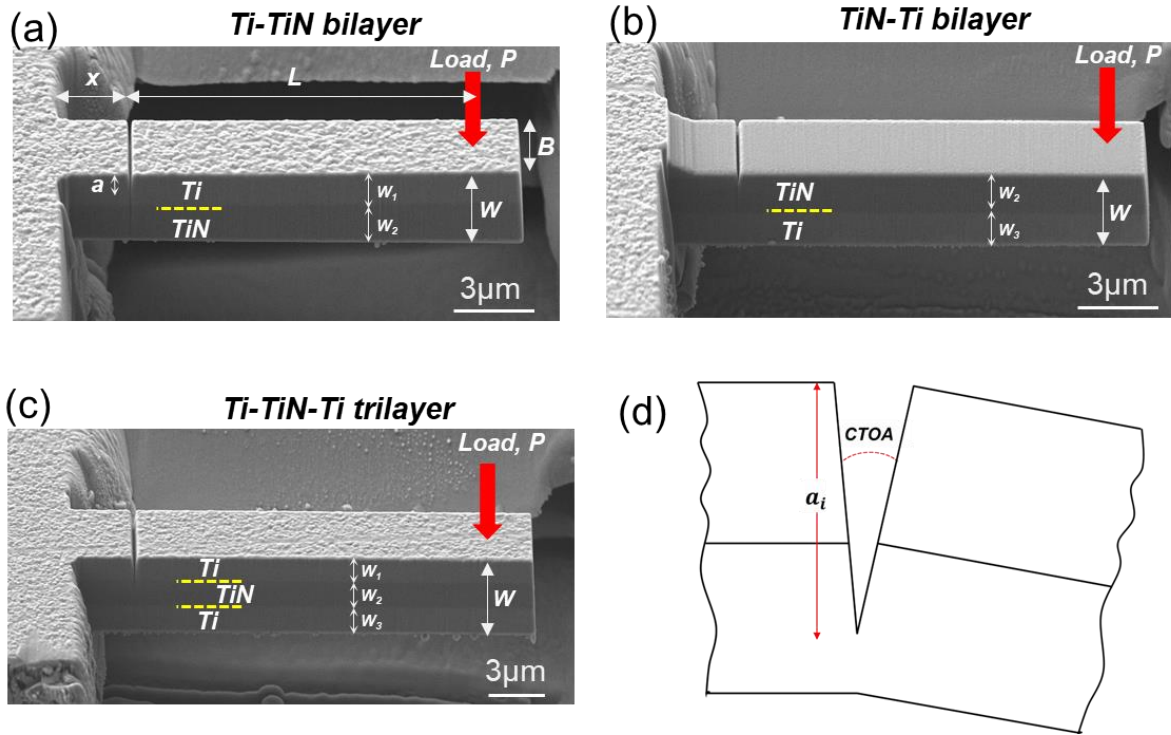


Fig. 1: Single edged notched microcantilever samples of a) Ti-TiN bilayer, b) TiN-Ti bilayer, and c) Ti-TiN-Ti trilayer system used for fracture testing. (Note: The initial notch was always positioned within the top layer). d) Schematic showing the measurement of crack tip opening angle for crack length 'a' at instant 'i'.

### 2.3 *Finite element simulations procedure*

The procedure to determine  $K_{IC}$  according to LEFM assumes a homogeneous material system, which is not strictly the case here. Hence, the crack driving force at the crack tip ( $J_{tip}$ ) developed during the microcantilever fracture experiments were estimated from finite element simulations using a two-dimensional model in ABAQUS CAE (Dassault Systemes Simulia Corp.). The material properties of the layers were assumed to be isotropic and homogeneous within the layer, with only elastic deformation in the TiN layer, whereas elastic-plastic deformation were considered for Ti layer with deformation plasticity incorporating Ramberg-Osgood plasticity model [18]. No properties were assigned to the interface, since earlier studies showed the interface to be sharp and adherent. The material properties used for Ti and TiN layers in the model have been reported in a previous study [6]. Boundary conditions of the cantilever were chosen such that the beams were encastered at one end without translations or rotations, while the other end was free to move in vertical direction. A wedge-shaped indenter was used to apply loads to the cantilever end. Surface-to-surface interaction was maintained with the outer surface of the indenter tip and the top surface of cantilever to ensure proper contact while loading. A stationary (non-propagating) crack was defined as a seam inside the cantilever. The crack driving forces were estimated using the contour integral approach with refined meshes near the crack tip as recommended by Treml et al. [19]. The simulations were performed for the following cases: i) Ti-TiN bilayer, ii) TiN-Ti bilayer, iii) Ti-TiN-Ti trilayer. Crack driving forces were extracted for an  $a/W$  of 0.3, 0.5 for the bilayer cantilevers and  $a/W$  of 0.3, 0.65 for the trilayer cantilever.

## 3 Results

### 3.1 *Microstructure of Ti-TiN thin film systems*

The GI-XRD pattern of the trilayer Ti-TiN-Ti thin film sample is shown in Fig. 2a. XRD pattern confirm the hexagonal phase of Ti and cubic phase of TiN from corresponding peak positions, and shows the polycrystalline nature of the layers. The intensity of the peaks for TiN are lower given that the layer is underneath the Ti, which is facing the X-ray beam. The ion channeling contrast image of the film cross-section as shown in Fig. 2b reveals the columnar growth pattern of the films and its nanocrystalline grain structure. A sharp and well adhered interface is visible with each individual layer of thickness of  $\sim 1.2 \mu\text{m}$ . Column sizes of approximately 22 nm for Ti and 50 nm for TiN films were estimated using the Scherrer formula [20], from the corresponding full width at half maximum (FWHM) of the (002) peak.

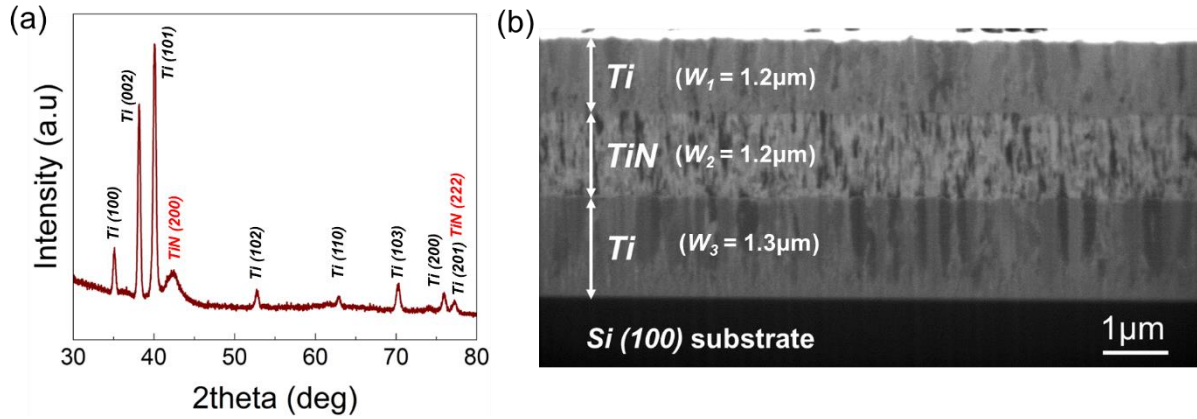


Fig. 2: a) Grazing incidence XRD pattern showing the phases of Ti (hexagonal) and TiN (cubic), and polycrystalline nature of films. b) Ion channeling image showing grain contrast of Ti-TiN-Ti trilayer film system.

### 3.2 Fracture behavior of bilayer and trilayer Ti-TiN systems

The representative load-displacement curves of the Ti-TiN bilayer, TiN-Ti bilayer and Ti-TiN-Ti trilayer microcantilever fracture tests are shown in Fig. 3a. All bilayer and trilayer systems showed an initial linear elastic response followed by a sharp load drop which corresponds to the crack propagation at the notch. The peak load was found to be the highest for the Ti-TiN-Ti trilayer, while for Ti-TiN and TiN-Ti bilayers the peak loads reached to less than 50% of the trilayer peak load. In the case of bilayer Ti-TiN, a complete brittle fracture of the whole system occurred as the crack propagated catastrophically across the brittle TiN layer without any crack arrest. In contrast to this, for the bilayer TiN-Ti system, the crack growth was arrested at TiN/Ti interface as the crack encountered a ductile Ti layer ahead. The load-displacement curve did not show a load drop to zero, unlike in the Ti-TiN case. Instead, a partial load shedding was followed by an increasingly non-linear deformation of the cantilever, due to the plastic zone expansion in the Ti layer. Both bilayer systems showed a similar slope in the initial elastic loading part as the combined stiffness remains the same in both configurations. This is different in case of Ti-TiN-Ti trilayer configuration, which showed a higher slope. Considering the overall width of the specimen being larger in this case, this is expected.

In Ti-TiN bilayer the crack propagates catastrophically in to the TiN layer in a linear elastic manner leading to complete fracture of the beam, whereas in the TiN-Ti and Ti-TiN-Ti systems, the crack propagates rapidly up to the TiN/Ti interface during the first load drop, post which the plastic zone in the Ti layer prevents it from further propagation, leading to gradual crack growth. This event corresponds to a larger load drop in the Ti-TiN-Ti trilayer, where the crack propagates across the entire TiN layer and reaches the next TiN/Ti interface, followed

by a non-monotonic rise in the load again due to crack tip stabilization. The initiation  $K_{IC}$  obtained in terms of LEFM based calculations using Eq. 2 and Eq. 3, for each system is listed in Table 1. Average  $K_{IC}$  of  $2.7 \pm 0.7 \text{ MPa}\cdot\text{m}^{0.5}$  for Ti-TiN,  $1.6 \pm 0.4 \text{ MPa}\cdot\text{m}^{0.5}$  for TiN-Ti, and  $3.2 \pm 1.0 \text{ MPa}\cdot\text{m}^{0.5}$  for Ti-TiN-Ti was estimated. The initiation  $K_{IC}$  values of Ti-TiN and Ti-TiN-Ti systems are comparable to the reported  $K_{IC}$  values of the individual Ti film ( $3.0 \pm 0.4 \text{ MPa}\cdot\text{m}^{0.5}$ ) [6], as the crack lay in the Ti layer in these cases, while that of the TiN-Ti system was closer to the individual TiN film ( $1.5 \pm 0.2 \text{ MPa}\cdot\text{m}^{0.5}$ ) [13,6].

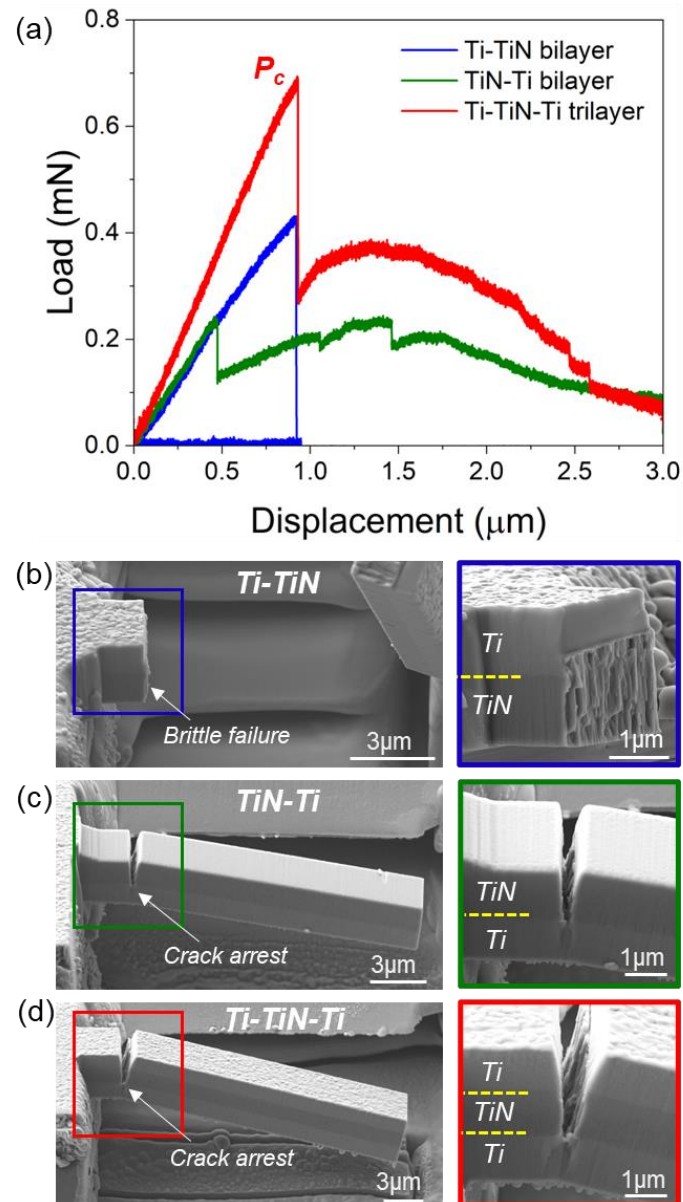


Fig. 3: a) Representative load-displacement curves showing the fracture behavior of different thin film systems during the microcantilever fracture experiments. Post fracture images of the microcantilevers showing b) brittle failure in Ti-TiN bilayer, crack arrest in c) TiN-Ti bilayer, and d) Ti-TiN-Ti trilayer system.

The post-fracture images of the Ti-TiN cantilever surface shown in Fig. 3b confirms the brittle fracture, as the crack propagated along the intercolumnar boundaries of the films of both Ti and TiN layers without any hinderance, whereas for the TiN-Ti and Ti-TiN-Ti systems, the plastic zone formation in the Ti layer ahead of the initial crack tip led to crack arrest and toughening, preventing complete fracture of the beam (Fig. 3c and 3d). Upon further bending the Ti layer deforms plastically and generates new nanocracks which then propagates into the Ti layer in both systems (Fig. 4). This pronounced plasticity at the notch tip needs to be evaluated using the J-integral approach. The iterative method of determining the plasticity contribution of J-integral solution using the unloading stiffness for each crack increment (as mentioned in [17]) is not used here as the system is not homogeneous, and shows abrupt, discrete load drops.

The critical displacement at initiation of fracture as measured from the microcantilever bending experiments was used to estimate the critical fracture energy for the two systems. The critical crack driving force ( $J_c$ ) values determined using Eq. 4 considering only the linear elastic regime of crack propagation is listed in Table 1. The initiation  $J_c$  values for Ti-TiN and TiN-Ti systems are found to be 44 N/m and 23 N/m respectively. The initiation  $J_c$  for the trilayer is determined to be 52 N/m. This  $J_c$  follows the same trend as a  $K_{IC}$ , which is as expected given the linear elastic regime of deformation at this stage. Further crack growth was quantified in terms of fracture resistance  $J_R$ . The Ti-TiN does not show any crack growth resistance at all, with catastrophic fracture ensuing post initiation. The pronounced plasticity at the crack tip near the Ti layer improves the  $J_R$  in TiN-Ti and Ti-TiN-Ti, which were estimated to be  $353 \pm 3$  N/m and  $498 \pm 33$  N/m respectively. Corresponding CTOA was found to be  $19^\circ$  and  $17^\circ$  respectively, indicating that  $J_R$  is a better measure to differentiate the fracture resistance between the two systems than CTOA.

*Table 1: Summary of the fracture resistance parameters obtained for each film system from microcantilever fracture tests.*

<b>Film system</b>	<b>Fracture toughness, <math>K_{IC}</math> from LEFM (<math>\text{MPa}\cdot\text{m}^{0.5}</math>)</b>	<b><math>J_c</math> from EPFM (N/m)</b>	<b><math>J_R</math> from EPFM (N/m)</b>	<b>Crack tip opening angle, CTOA (<math>^\circ</math>)</b>
Ti-TiN with crack in Ti	$2.7 \pm 0.7$	$44 \pm 6$	$44 \pm 6$	-
TiN-Ti with crack in TiN	$1.6 \pm 0.4$	$23 \pm 1$	$353 \pm 3$	$19 \pm 2.0$
Ti-TiN-Ti with crack in Ti	$3.2 \pm 1.0$	$52 \pm 16$	$498 \pm 33$	$17 \pm 0.2$

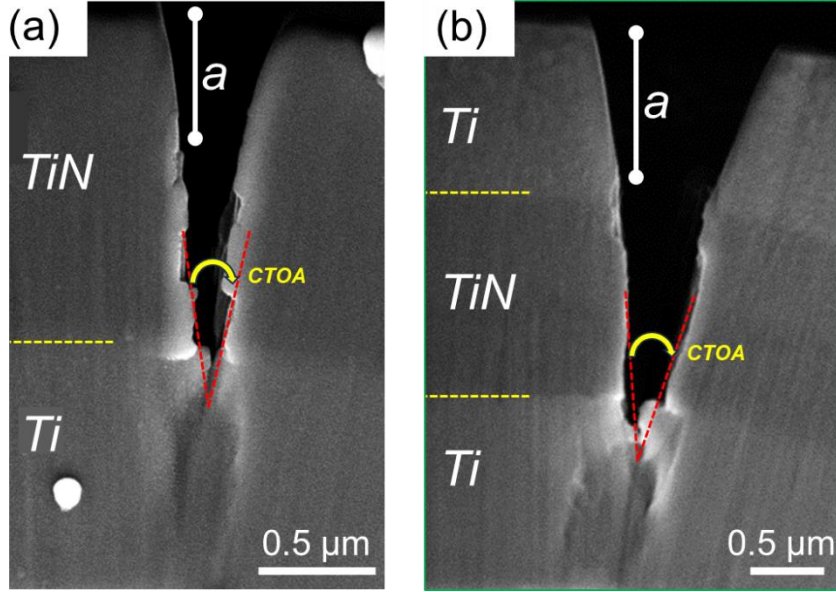


Fig. 4: Crack arrest and plastic zone development in Ti layers in a) Ti-TiN and b) Ti-TiN-Ti systems at maximum displacement of the cantilever (with crack tip opening angle marked in red lines).

#### 4 Discussion

The crack tip driving force ( $J_{tip}$ ) curve as a function of the cantilever displacement is shown in Fig. 5a. For a fixed displacement, the TiN-Ti has a higher  $J_{tip}$  compared to the Ti-TiN system, which explains the lower initiation fracture toughness of the former. The crack driving force decreases as the crack propagates towards TiN, whereas there is an increase when the crack grows towards Ti. The trilayer experiences the lowest crack driving force amongst all. This is along the expected lines of the crack tip shielding and anti-shielding effects due to the elastic modulus mismatch between the layers. On comparing the fracture resistance parameters of bilayer Ti-TiN and TiN-Ti systems as shown in Table 1, the crack located in the Ti layer (for Ti-TiN) shows higher initiation resistance (from the corresponding  $K_{IC}$  values) compared to the case of crack in TiN layer (for TiN-Ti). This is expected given that the  $K_{IC}$  of single layer Ti is almost double that of the TiN layer [6]. In comparison to single layer Ti,  $K_{IC}$  of Ti-TiN is 10% lower, reinforcing that the elastic shielding effect of the TiN layer ahead of the crack tip plays an insignificant role, while truncation of crack tip plasticity in fact reduces the initiation  $K_{IC}$  of the bilayer. In fact a stiffer layer resists the expansion of the plastic zone in the Ti layer even more. On the other hand, the  $K_{IC}$  of TiN-Ti is ~7% higher than the single layer TiN, since a softer Ti ahead of the crack tip allows for relaxing the stress intensification in the TiN. The  $K_{IC}$  of the trilayer is not compromised since to the the shielding effect of the TiN is

countered by the crack tip plasticity in the third Ti layer. Thus the trilayer offers a 16% increase in  $K_{IC}$  compared to the single layer Ti.

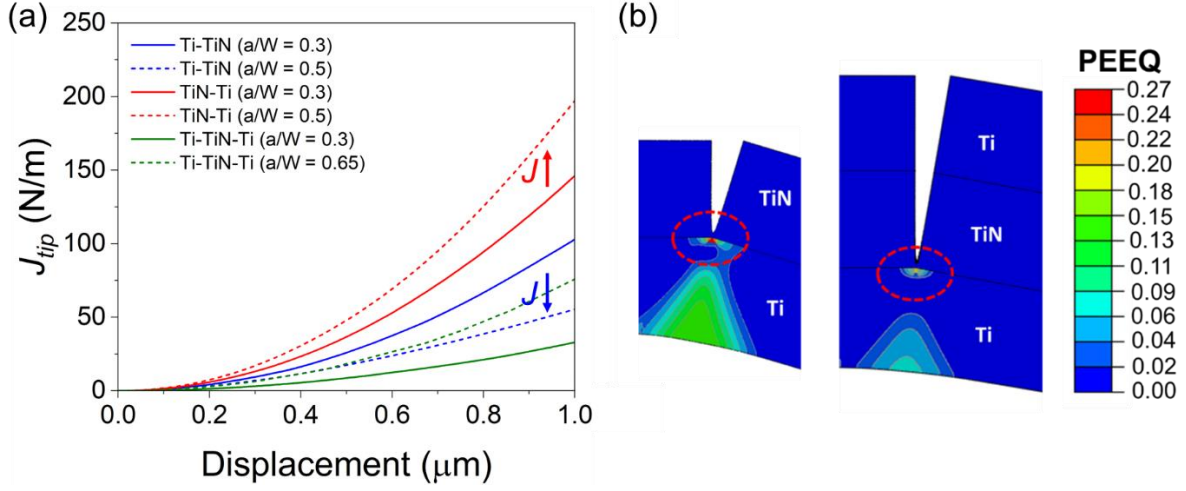


Fig. 5: a) Crack tip driving force variation with cantilever displacement Ti-TiN, TiN-Ti and Ti-TiN-Ti systems from finite element simulations assuming non propagating cracks. b) Plastic zone evolution near the crack tip (in red circles) in the Ti layer (shown as plastic energy equivalent-PEEQ) in TiN-Ti bilayer and Ti-TiN-Ti trilayer system when the crack meets the TiN/Ti interface.

In both bilayer configurations, the crack once initiated, extends rapidly towards the second layer until it encounters the interface, upon which the fracture behavior diverges for the two cases. Further crack propagation depends on the ductile or brittle nature of the next layer ahead. The  $R$ -curve in the bilayer TiN-Ti and the trilayer Ti-TiN-Ti is made possible due to a fully developed plastic zone in the Ti layer once the crack reaches the TiN/Ti interface. The plastic zone size is found to be of the order of 124 nm in the TiN-Ti bilayer and 170 nm in the Ti-TiN-Ti systems as shown in Fig. 5b, when the crack reaches that interface, due to which the crack tip undergoes significant blunting. In addition, the plasticity due to the compressive stresses on the other side of the beam, extending almost to connect to the crack tip process zone, also leads to toughening and preventing further crack growth. When the Ti layer is reduced in thickness so as to truncate its plastic zone to less than 100 nm, such an  $R$ -curve behavior is not observed anymore [6]. This is seen in the case of the bilayer Ti-TiN, where the available distance ahead of the crack tip in the Ti layer is insufficient to provide significant crack tip plasticity. In case of the trilayer, the initial crack experiences a shielding effect due to the TiN layer ahead of it, and as the crack propagates to the TiN/Ti interface, it experiences toughening due to the crack tip plasticity in the Ti layer. Therefore, the trilayer is able to synergistically blend the advantages of elastic and plastic shielding to give the highest toughening. The

quantification of the *R*-curve in such systems will help in design of multilayer and graded architectures with improved fracture resistance.

## 5 Conclusions

The fracture behavior of bilayered and trilayered Ti-TiN multilayered film systems were studied using microcantilever fracture tests to understand the fundamental crack growth mechanisms in hard coatings. The initiation fracture toughness values of  $2.7 \pm 0.7 \text{ MPa}\cdot\text{m}^{0.5}$  and  $1.6 \pm 0.4 \text{ MPa}\cdot\text{m}^{0.5}$  were found for Ti-TiN and TiN-Ti layers, similar to  $K_{IC}$  of monolithic Ti and TiN respectively. More importantly, it was shown that including a Ti layer ahead of the crack tip leads to a rising fracture resistance, with the plastic dissipation in the Ti layer preventing catastrophic fracture, in TiN-Ti bilayer and Ti-TiN-Ti trilayer systems, unlike in the case of Ti-TiN bilayer. This dictates that the position of the crack tip and type of layer ahead of it determines the fracture behavior. The results show that the influence of elastic shielding ahead of the crack tip plays an antagonistic role in suppressing crack tip plasticity in initiation toughness, but plastic shielding does impact propagation resistance. Using this information, multilayer Ti-TiN system can be designed using Ti with minimum thickness to provide process zone toughening while not impacting the hardness of the system. Graded multilayers with a harder surface and a tougher interior can be designed based on this study, so as to exploit the advantage of resisting crack growth as fracture initiates from the surface and proceeds towards the interior.

### **CRedit authorship contribution statement**

**Nidhin George Mathews:** Conceptualization, Methodology, Data curation, Formal Analysis, Investigation, Visualization, Writing – original draft, Writing – review & editing. **Aloshious Lambai:** Methodology. **Marcus Hans:** Methodology, Writing – review & editing. **Jochen M. Schneider:** Methodology, Writing – review & editing. **Gaurav Mohanty:** Supervision, Funding Acquisition, Writing – original draft, Writing – review & editing. **Balila Nagamani Jaya:** Conceptualization, Supervision, Writing – original draft, Writing – review & editing.

### **Declaration of Competing Interest**

The authors declare that they have no known competing financial interests or personal relationships that could have appeared to influence the work reported in this paper.

## Acknowledgements

Authors acknowledge the Research Council of Finland (grant no. 341050) for financial support. The work made use of facilities at Tampere Microscopy Center at Tampere University.

## References

- [1] S. Zhang, W. Zhu, TiN coating of tool steels: a review, *Journal of Materials Processing Technology* 39 (1993) 165–177. [https://doi.org/10.1016/0924-0136\(93\)90016-Y](https://doi.org/10.1016/0924-0136(93)90016-Y).
- [2] M. Larsson, M. Bromark, P. Hedenqvist, S. Hogmark, Deposition and mechanical properties of multilayered PVD Ti–TiN coatings, *Surface and Coatings Technology* 76–77 (1995) 202–205. [https://doi.org/10.1016/0257-8972\(95\)02589-8](https://doi.org/10.1016/0257-8972(95)02589-8).
- [3] K.J. Ma, A. Bloyce, T. Bell, Examination of mechanical properties and failure mechanisms of TiN and Ti–TiN multilayer coatings, *Surface and Coatings Technology* 76–77 (1995) 297–302. [https://doi.org/10.1016/0257-8972\(95\)02585-5](https://doi.org/10.1016/0257-8972(95)02585-5).
- [4] H.H. Mofidi, A.S. Rouhaghdam, S. Ahangarani, M. Bozorg, M. Azadi, Fracture Toughness of TiN Coating as a Function of Interlayer Thickness, *Advanced Materials Research* 829 (2014) 466–470. <https://doi.org/10.4028/www.scientific.net/AMR.829.466>.
- [5] C.L. Jiang, H.L. Zhu, K.S. Shin, Y.B. Tang, Influence of titanium interlayer thickness distribution on mechanical properties of Ti/TiN multilayer coatings, *Thin Solid Films* 632 (2017) 97–105. <https://doi.org/10.1016/j.tsf.2017.04.026>.
- [6] A.K. Mishra, H. Gopalan, M. Hans, C. Kirchlechner, J.M. Schneider, G. Dehm, B.N. Jaya, Strategies for damage tolerance enhancement in metal/ceramic thin films: Lessons learned from Ti/TiN, *Acta Materialia* 228 (2022) 117777. <https://doi.org/10.1016/j.actamat.2022.117777>.
- [7] M.B. Daia, P. Aubert, S. Labdi, C. Sant, F.A. Sadi, Ph. Houdey, J.L. Bozet, Nanoindentation investigation of Ti/TiN multilayers films, *Journal of Applied Physics* 87 (2000) 7753–7757. <https://doi.org/10.1063/1.373450>.
- [8] T. Mori, S. Fukuda, Y. Takemura, Improvement of mechanical properties of Ti/TiN multilayer film deposited by sputtering, *Surface and Coatings Technology* 140 (2001) 122–127. [https://doi.org/10.1016/S0257-8972\(01\)01021-0](https://doi.org/10.1016/S0257-8972(01)01021-0).
- [9] T.S. Li, H. Li, F. Pan, Microstructure and nanoindentation hardness of Ti/TiN multilayered films, *Surface and Coatings Technology* 137 (2001) 225–229. [https://doi.org/10.1016/S0257-8972\(00\)01096-3](https://doi.org/10.1016/S0257-8972(00)01096-3).
- [10] K. Matoy, H. Schönherr, T. Detzel, T. Schöberl, R. Pippan, C. Motz, G. Dehm, A comparative micro-cantilever study of the mechanical behavior of silicon based

- passivation films, *Thin Solid Films* 518 (2009) 247–256.  
<https://doi.org/10.1016/j.tsf.2009.07.143>.
- [11] J. Ast, M. Ghidelli, K. Durst, M. Göken, M. Sebastiani, A.M. Korsunsky, A review of experimental approaches to fracture toughness evaluation at the micro-scale, *Materials & Design* 173 (2019) 107762. <https://doi.org/10.1016/j.matdes.2019.107762>.
- [12] S. Massl, W. Thomma, J. Keckes, R. Pippan, Investigation of fracture properties of magnetron-sputtered TiN films by means of a FIB-based cantilever bending technique, *Acta Materialia* 57 (2009) 1768–1776. <https://doi.org/10.1016/j.actamat.2008.12.018>.
- [13] R. Daniel, M. Meindlhuber, W. Baumegger, J. Zalesak, B. Sartory, M. Burghammer, C. Mitterer, J. Keckes, Grain boundary design of thin films: Using tilted brittle interfaces for multiple crack deflection toughening, *Acta Materialia* 122 (2017) 130–137.  
<https://doi.org/10.1016/j.actamat.2016.09.027>.
- [14] J. Buchinger, L. Löfler, J. Ast, A. Wagner, Z. Chen, J. Michler, Z.L. Zhang, P.H. Mayrhofer, D. Holec, M. Bartosik, Fracture properties of thin film TiN at elevated temperatures, *Materials & Design* 194 (2020) 108885.  
<https://doi.org/10.1016/j.matdes.2020.108885>.
- [15] N.G. Mathews, A.K. Mishra, B.N. Jaya, Mode dependent evaluation of fracture behaviour using cantilever bending, *Theoretical and Applied Fracture Mechanics* 115 (2021) 103069. <https://doi.org/10.1016/j.tafmec.2021.103069>.
- [16] B.N. Jaya, V. Jayaram, Crack stability in edge-notched clamped beam specimens: modeling and experiments, *Int J Fract* 188 (2014) 213–228.  
<https://doi.org/10.1007/s10704-014-9956-2>.
- [17] S. Wurster, C. Motz, R. Pippan, Characterization of the fracture toughness of micro-sized tungsten single crystal notched specimens, *Philosophical Magazine* 92 (2012) 1803–1825. <https://doi.org/10.1080/14786435.2012.658449>.
- [18] W. Ramberg, W.R. Osgood, Description of stress-strain curves by three parameters, (1943). <https://ntrs.nasa.gov/citations/19930081614> (accessed January 7, 2025).
- [19] R. Treml, D. Kozic, R. Schöngrundner, O. Kolednik, H.-P. Gänser, R. Brunner, D. Kiener, Miniaturized fracture experiments to determine the toughness of individual films in a multilayer system, *Extreme Mechanics Letters* 8 (2016) 235–244.  
<https://doi.org/10.1016/j.eml.2016.01.004>.
- [20] P. Scherrer, Bestimmung der Größe und der inneren Struktur von Kolloidteilchen mittels Röntgenstrahlen, *Nachrichten von der Gesellschaft der Wissenschaften zu Göttingen, Mathematisch-Physikalische Klasse* 1918 (1918) 98–100.